Rare Metal Materials and Engineering
Volume 55, Issue 8, August 2026
Available online at www.rmme.ac.cn

Science Press

Cite this article as: Feng Jingru, Zhang Kezhao, Liu Dong, et al. Microstructural Evolution and Heterogeneous Precipitation of Laser Welded TB9 Alloy Joints[J]. Rare Metal Materials and Engineering, 2026, 55(08): 1897-1906. DOI: https://doi.org/10.12442/j.issn.1002-185X.20250479.

ARTICLE

Microstructural Evolution and Heterogeneous Precipitation of Laser Welded TB9 Alloy Joints

Feng Jingru, Zhang Kezhao, Liu Dong, Yan Chunyan, Cheng Jiangbo, Bao Yefeng

College of Materials Science and Engineering, Hohai University, Changzhou 213200, China

Abstract: The microstructural evolution during the laser welding and subsequent post-weld heat treatment processes of laser welded TB9 joints was investigated. Results show that, during the laser welding process, the average size of β grains in the fusion zone increases with the increase in laser power. During the aging treatment, the size of the α phase increases with the increase in temperature. Concurrently, the quantity of the α phase decreases. The size of the α phase also increases with the prolongation of holding time. Meanwhile, the morphology of α phase transforms from a needle-like structure to an elliptical one. After the heat treatments, the precipitation-free zones (PFZs) are observed in the fusion zone, heat-affected zone (HAZ), and base metal of the welded joint. The formation of PFZs is due to the inhomogeneous precipitation and growth of α phase. PFZs exist between the dendrite arms in the fusion zone, near the grain boundaries in HAZ, and near the low angle grain boundaries (LAGBs) and grain boundaries of the base metal. In the fusion zone, the formation of PFZs is due to the enrichment of element Cr between dendrite arms. In HAZ and base metal, the formation of PFZs is attributed to vacancy depletion around grain boundaries as well as LAGBs.

Key words: β titanium alloy; laser welding; α precipitation; PFZ

1 Introduction

Titanium alloys are well known for their low density, excellent mechanical performance, and superior oxidation and corrosion resistance. Due to these advantages, titanium alloys are widely used in aerospace, aviation, ocean, and biomedical engineering fields[1–3]. With the addition of different elements, titanium alloys can be roughly divided into α, $\alpha+\beta$, and β titanium alloys. TB9 alloy belongs to the metastable β titanium alloy among the above-mentioned three categories. It can be used for manufacturing fasteners in aerospace engineering. The welding techniques of TB9 alloy and other β titanium alloys involve linear friction welding, electron beam welding, and arc welding[4–6]. Laser welding is also often used for the welding of titanium alloys, particularly in aerospace engineering, due to its low heat input and high efficiency[7–8]. It has been discovered that the fusion zone of laser welded β titanium alloys is usually composed of full β phase because of the presence of a large amount of β-stabilizing elements. Due to the lack of strengthening phases in the fusion zone, the tensile strength of laser welded β titanium alloys is reduced. Appropriate post-weld heat treatment is essential for laser welded β titanium alloys.

Although there are currently many studies focusing on the influence of heat treatment on the microstructure and properties of TB9 alloys, research focused on laser welded TB9 joints is relatively restricted. Yang et al[9] studied the distribution of temperature, stress, and strain of TB9 alloy during the linear friction welding process using the finite element method. The microstructure in the different regions of the joints was also verified. For other β titanium alloys, such as TB8 prepared by laser welding, $\beta\rightarrow\omega$ or $\beta\rightarrow\alpha$ occurs dependently on the temperature of aging treatment[10]. It is to be noted that, due to the difference in the primary microstructures of the fusion zone, heat-affected zone (HAZ), and base metal of alloys at the as-welded state, the precipitation behavior of α phase varies in these regions. Moreover, the thermal cycles during welding process lead to the redistribution of constituent elements and microstructural evolution in the fusion zone and HAZ, which has an influence

Received date: September 19, 2025
Foundation item: Fundamental Research Funds for the Central Universities of China (B220202026); Changzhou Sci&Tech Program (CJ20220074)
Corresponding author: Zhang Kezhao, Ph. D., Associate Professor, College of Materials Science and Engineering, Hohai University, Changzhou 213200, P. R. China, E-mail: zhangkz@hhu.edu.cn

on the precipitation of α phase. On account of the above-mentioned reasons, it is essential to investigate the inhomogeneous microstructure in the different regions of the joints after heat treatment. Previous investigations discussed the nonuniform precipitation of α phase during heat treatment in TB9 alloy, but the difference in microstructure in the different regions of laser welded TB9 joints was seldom reported[11–12].

The influence of post-weld heat treatment on the microstructural evolution of laser welded TB9 joints was investigated, focusing on the inhomogeneous precipitation of α phase in the different regions. The relationship between the precipitation behavior of α phase and the primary microstructure, as well as the distribution of constituent elements, was discussed. The aim is to provide a deep understanding of the microstructural evolution during the heat treatment and a reference for developing a proper heat treatment process of laser welded TB9 joints.

2 Experiment

The base metal used for the laser welding process was hot-rolled rods with a diameter of 45 mm. The chemical composition of TB9 alloy is shown in Table 1. The microstructure of the as-received base metal is shown in Fig.1. The microstructure is primarily composed of β phase with residual α phase, which is attributed to the hot rolling process at the temperature of β phase field. Before welding, the rod was cut into smaller plates with a thickness of 2 mm. The plates were subsequently ground to remove the traces left by wire electric discharge machining.

Heat input can be calculated directly from Eq. (1). The welding parameters are shown in Table 2. After welding, a series of heat treatments were conducted on the laser welded joints. The parameters of post-weld heat treatments are shown in Table 3.

$$\text{Heat input} = \frac{P}{v} \quad (1)$$

Table 1 Chemical composition of base metal (wt%)

Al	V	Cr	Mo	Zr	Fe	Ti
3.54	8.18	6.08	4.01	4.13	0.05	Bal.

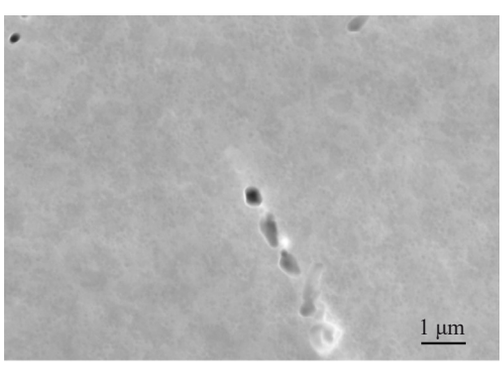

Fig.1 Microstructure of base metal

Table 2 Parameters for laser welding process

Laser power, P/W	Welding speed, v/m·min^{-1}	Heat input/J·mm^{-1}
800	1	48
1000	1	60
1200	1	72

Table 3 Parameters of heat treatments

Sample	Aging temperature/℃	Holding time/h	Cooling
400-8	400	8	
500-8	500	8	
600-8	600	8	Air cooling
400-24	400	24	(AC)
500-24	500	24	
600-24	600	24	

where P is laser power (W), and v is welding speed (m/min). The unit of heat input is J/mm.

The samples for microstructure analysis were cut out from the welded plates using wire electric discharge machining. The metallographic samples were cut out perpendicular to the welding direction. These samples were then polished and etched with a Kroll's solution of 5% HF, 35% HNO_3, and 60% water. The optical microscope (OM, Axiolab 5) was used to observe the overall macrostructural characteristics, and the scanning electron microscope (SEM, Gemini 300) with energy dispersive spectrometer (EDS) was used to analyze the microstructural characteristics, such as the size and morphology of α phase and β phase. The samples for electron back scattered diffractometer (EBSD, Symmetry S2) were further electropolished to observe the grain morphology, grain size, and misorientation angle distribution of β phase. The samples for transmission electron microscope (TEM, Tecnai G2 F20) were polished and then ion-milled to a thickness of 30–40 μm in order to analyze the dimensions of α phase and β phase. The electron probe microanalyzer (EPMA, 1720H) test was used to conduct element quantitative analysis in the different regions of laser welded TB9 joints. The muffle furnace TCXC1700 was selected to conduct the heat treatments with a control accuracy of ±1 ℃. The samples for heat treatments were encapsulated in quartz tubes filled with argon gas.

3 Results and Discussion

3.1 Microstructure

The microstructure of the welded joints is shown in Fig.2. It is difficult to distinguish the boundary between fusion zone, HAZ, and base metal, because the constituent phase in these regions is dominantly β phase. In laser welded α and $\alpha+\beta$ titanium alloys, such as TA15 and TC4, the phase transformation sequence is $\alpha \rightarrow \beta \rightarrow \alpha'$[13]. By contrast, in laser welded β titanium alloys, the $\beta \rightarrow \alpha'$ martensitic transformation is suppressed because the β titanium alloys usually contain

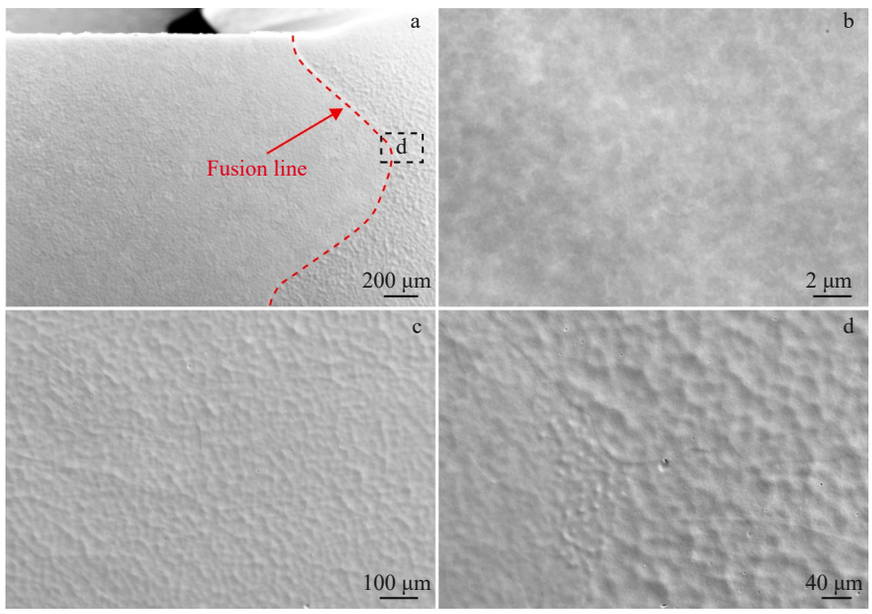

Fig.2 Microstructures of laser welded TB9 alloy: (a) overall microstructure; (b) HAZ; (c–d) fusion zone

much higher amount of β-stabilizing elements[6–7]. The $[Mo]_{eq}$ (molybdenum equivalency) is often used to measure the level of β-stabilizing elements in β titanium alloys. In general, as the $[Mo]_{eq}$ is higher than 10%, the $\beta \rightarrow \alpha'$ martensitic transformation can be completely suppressed during the fast cooling process, such as quenching and fusion welding[14]. The calculated $[Mo]_{eq}$ of TB9 alloy using Eq. (2) [15] is approximately 20%, indicating that the full β microstructure is achievable in HAZ and fusion zone, as shown in Fig. 2b and Fig. 2c–2d, respectively. The primary microstructure of base metal is also mostly composed of β phase, as presented in Fig. 1. Therefore, the joints are predominantly composed of the β phase with a small amount of second phases.

$$[Mo]_{eq} = Mo + \frac{Nb}{3.3} + \frac{Ta}{4} + \frac{W}{2} + \frac{Cr}{0.6} + \frac{Mn}{0.6} + \frac{V}{1.4} + \frac{Fe}{0.5} + \frac{Co}{0.9} + \frac{Ni}{0.8} \quad (2)$$

Since the different regions of laser welded joints present similar constituent phases, EBSD was used to characterize the grain morphology. The influence of laser power on the microstructure of the joints is shown in Fig. 3. It can be seen that the width of fusion zone increases with the increase in laser power. The β grains in the fusion zone exhibit symmetrical columnar morphology due to the large temperature gradient caused by the laser beam, while the grains in base metal and HAZ are basically equiaxed, as shown in Fig. 3. As the laser power reaches 1200 W, some equiaxed β grains are found in the center of fusion zone, as indicated in Fig. 3c. The formation of equiaxed grains in the fusion zone is closely related to the temperature gradient of the welding pool during solidification. The higher the laser power, the smaller the temperature gradient, driving the grain growth mode changing from cellular dendritic growth to equiaxed dendritic growth, and resulting in the formation of equiaxed grains in the fusion zone, as shown in Fig. 3c. The

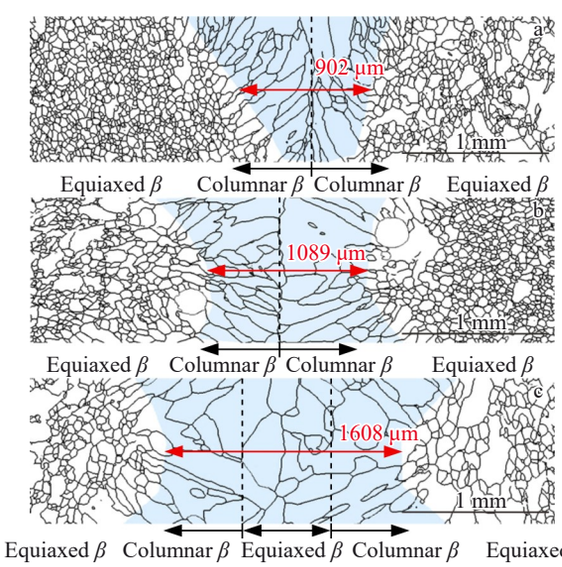

Fig.3 EBSD analysis of laser welded TB9 joints under different laser powers: (a) 800 W; (b) 1000 W; (c) 1200 W

selected fusion zone for the calculation of the average grain size is indicated in light blue color. As the laser power increases from 800 W to 1200 W, the average grain size is 87, 96, and 119 μm, respectively. Therefore, the higher heat input promotes the growth of β grains during solidification.

3.2 Influence of heat treatment on microstructure

The influence of temperature and holding time on the microstructure of the fusion zone is shown in Fig. 4. It can be seen that the fraction and morphology of α phase change with different heat treatment conditions. As the temperature increases, there is a corresponding increase in the size of α phase. The α phase morphology of the 400-8 sample is needle-shaped with very small width, as shown in Fig. 4a. By comparison, the length and width of the α phase of 500-8 and 600-8 samples are much larger, as shown in Fig. 4c and Fig. 4e.

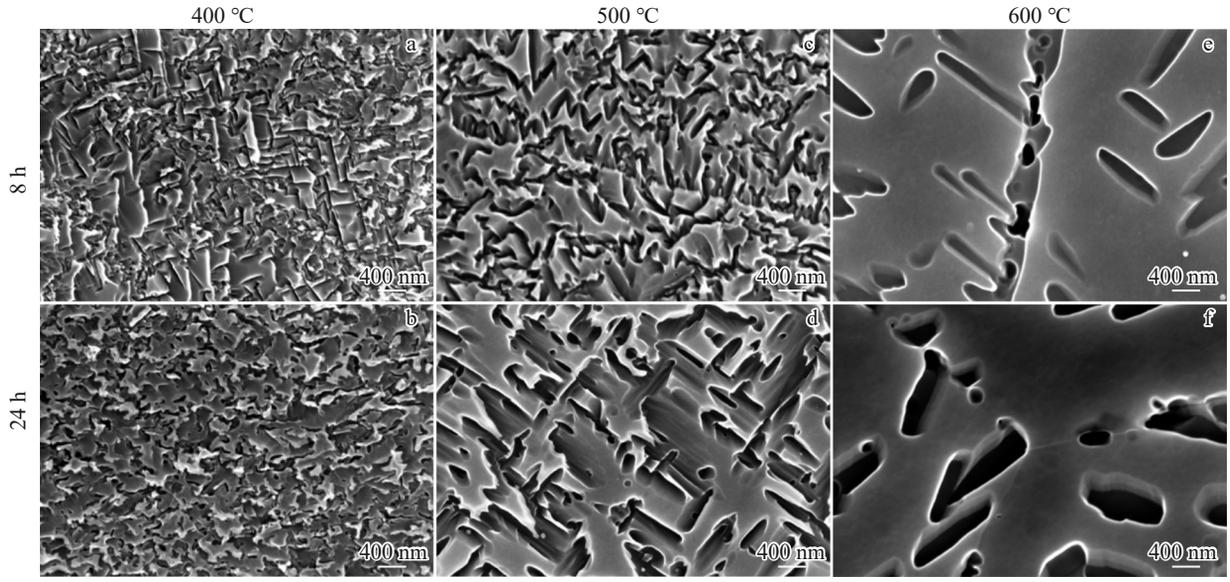

Fig.4 Microstructures in fusion zone of samples with different heat treatments: (a) 400-8; (b) 400-24; (c) 500-8; (d) 500-24; (e) 600-8; (f) 600-24

At the same time, it can be seen that the amount of *α* phase decreases as the temperature increases from 400 ℃ to 600 ℃. The influence of holding time of heat treatment on the microstructure can be observed from the increased size of *α* phase as the holding time increases from 8 h to 24 h.

The microstructural evolution in HAZ after the heat treatment is shown in Fig. 5. The morphology and size of *α* phase in HAZ present similar trends to those in the fusion zone, as the temperature and holding time change. It is found that the *α* phase tends to distribute along the grain boundary at 600 ℃, as shown in Fig.5e–5f.

The influence of heat treatment on the microstructure of base metal is shown in Fig. 6. The morphology and size of *α* phase in base metal change similarly to those in fusion zone and HAZ. It is noteworthy that some *α* precipitates are distributed in a chain-like pattern within the grains, as shown in Fig.6a–6b.

TEM analysis of fusion zone was also conducted to investigate the influence of heat treatment on the microstructure, as shown in Fig.7.

Generally speaking, the size of *α* phase increases with the increase in temperature and holding time during heat treatment. The width of the *α* phase of samples with different heat treatments, calculated from Fig.7, is shown in Table 4.

The *α* phase in the different regions of laser welded TB9 joints presents similar change features during the heat treatment. In general, the size of *α* phase increases with the increase in temperature, while the quantity decreases. Meanwhile, the morphology of *α* phase changes from needle-shaped to elliptical. This phenomenon is mainly dependent on

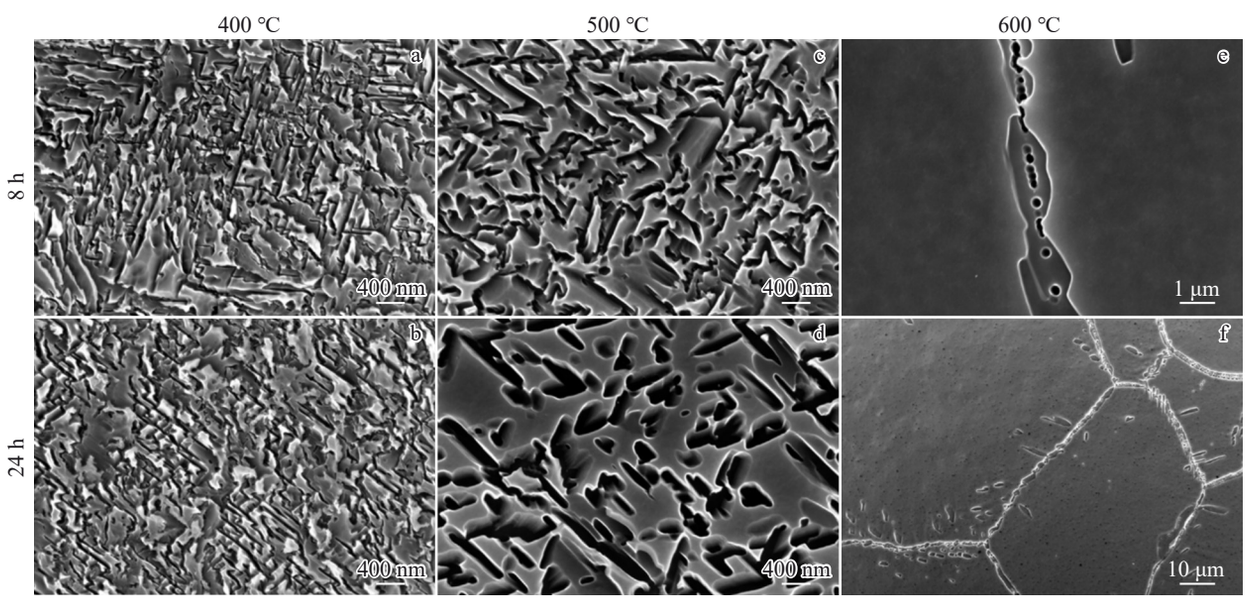

Fig.5 Microstructures in HAZ of samples with different heat treatments: (a) 400-8; (b) 400-24; (c) 500-8; (d) 500-24; (e) 600-8; (f) 600-24

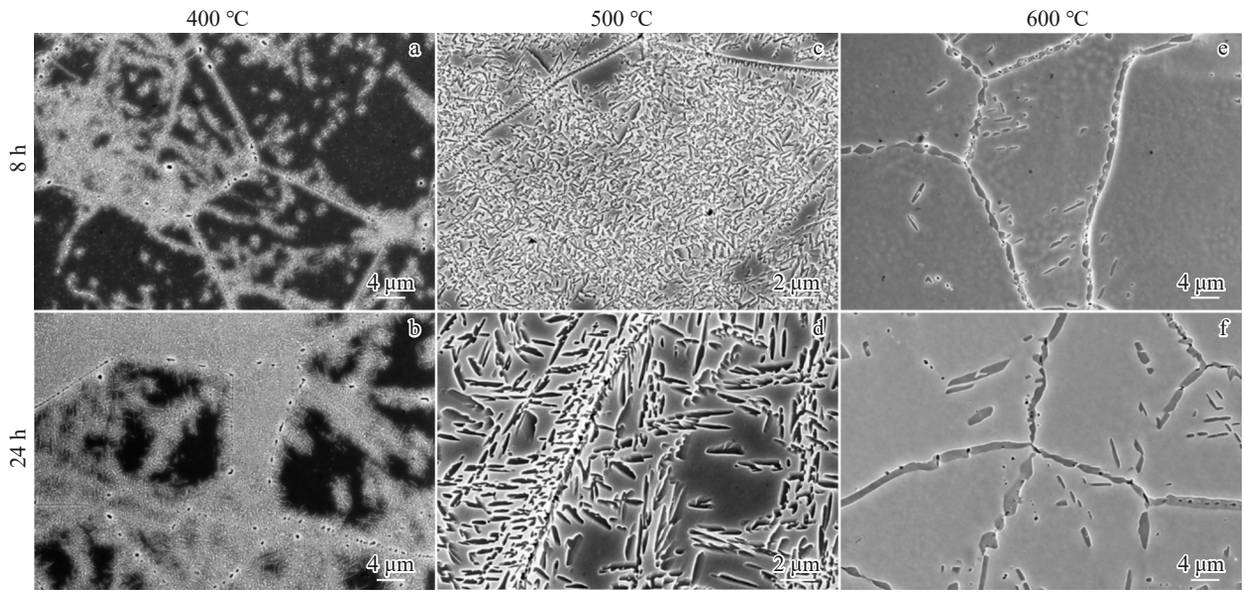

Fig.6 Microstructures in base metal of samples with different heat treatments: (a) 400-8; (b) 400-24; (c) 500-8; (d) 500-24; (e) 600-8; (f) 600-24

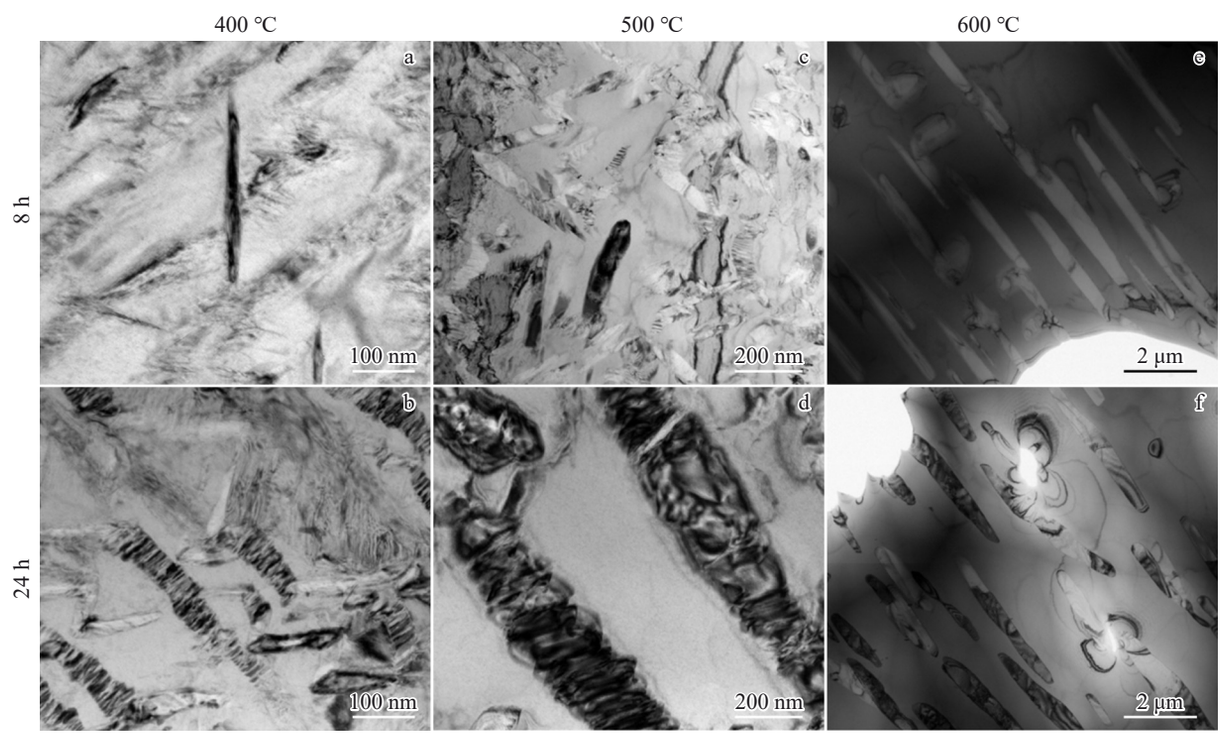

Fig.7 TEM images in fusion zone of samples with different heat treatments: (a) 400-8; (b) 400-24; (c) 500-8; (d) 500-24; (e) 600-8; (f) 600-24

Table 4 α phase width of samples with different heat treatments

Sample	Width/nm
400-8	22.1±3.3
500-8	95.5±8.5
600-8	546.5±66.7
400-24	54.1±9.6
500-24	263.2±14.8
600-24	689.5±73.6

the nucleation and growth mechanism of α phase. The formation of α phase of sample heat-treated at lower temperatures (usually below 400 ℃) is often related to the $\beta \rightarrow \omega$ transformation. The formation of ω phase leads to the uneven distribution of elements and promotes the nucleation of α phase. By comparison, the α phase nucleates directly within the β matrix at higher temperatures (usually above 500 ℃). The growth of α phase requires the diffusion of α- and β-stabilizing elements, and hence, the higher temperature and longer holding time can promote the growth of α phase.

The inhomogeneous distribution of α phase is observed in

the different regions of laser welded TB9 joints. There exist precipitation free zones (PFZs) in the joints after the heat treatments. PFZs refer to regions with a much lower density of α phase. The distribution of α phase in the fusion zone, HAZ, and base metal after the heat treatments is shown in Fig. 8. Since the β phase has better corrosion resistance than the α phase, the bright regions indicate that a lower fraction of α phase exists. The brightest regions can be defined as PFZs. By contrast, the darker regions contain a larger amount of α phase. It can be seen that the distribution of PFZs also varies with the different areas of the joints. In fusion zone, the morphology of PFZs presents the features related to the grain growth of β grains, as observed in Fig. 8a–8c. In HAZ, PFZs mainly locate at the grain boundary, as shown in Fig.8d–8e. In base metal, a fraction of α phase is concentrated and distributed in a chain-like morphology around PFZs, as indicated in Fig.8g–8i.

The influence of holding time on the distribution of PFZ is shown in Fig. 9. Generally speaking, the longer holding time of heat treatment can promote the formation of more α phase and reduce the size and amount of PFZs. When the holding time of heat treatment increases to 24 h, the formation of PFZs is effectively suppressed, especially in fusion zone, as can be seen from Fig.8a–8c and Fig.9a–9c.

The 500-8 sample is used to investigate the reason for the formation and distribution of PFZs in the different regions of the joints. The morphology of PFZs in the fusion zone and its corresponding EDS element mapping analysis of 500-8 sample is shown in Fig. 10. The results show that the distribution of PFZs in fusion zone is related to elemental segregation. The morphology of PFZs is shown in Fig. 10a. PFZs mainly locate in the Cr-rich and Mo-lean regions, as seen in Fig. 10b and Fig. 10c, respectively. Meanwhile, elements Al and V are homogeneously distributed in both PFZs and non-PFZs.

The detailed morphology of PFZs in HAZ is shown in Fig.11a. As depicted in Fig.8d–8f, PFZs are mainly distributed adjacent to the grain boundary, and the size is small. The distribution of elements Cr, Mo, Al, and V is generally uniform, as shown in Fig.11b–11e.

The morphology of PFZs in base metal is quite different from that in fusion zone and HAZ. The α phase precipitates in a chain-like pattern, as shown in Fig. 12a. No obvious segregation of elements Cr, Mo, Al, and V is found, as shown in Fig. 12b – 12e. The formation of PFZs is supposed to be related to the low angle grain boundaries (LAGBs) formed during the rolling process of base metal, as shown in Fig.13.

The results presented above show that there exist PFZs in the fusion zone, HAZ, and base metal of laser welded TB9 joints. The formation of PFZs is also found in other alloys. The main reasons are attributed to the solute depletion, vacancy depletion, or the combined effects of both[16]. The schematic diagrams of the formation of PFZs in fusion zone, HAZ, and base metal is shown in Fig. 14. PFZs in the fusion zone show an obvious connection with the segregation of elements Cr and Mo, as shown in Fig. 14a. By contrast, there is no obvious segregation of α-stabilizing (Al) and β-stabilizing (Cr, Mo, V) elements in PFZs of the HAZ and base metal, as shown in Fig.14b and 14c, respectively. For PFZs in fusion zone, the formation of Cr-rich and Mo-lean PFZs is attributed to the different partition coefficients of elements Mo and Cr during the solidification process. The partition coefficient of element Mo is higher than 1, while that

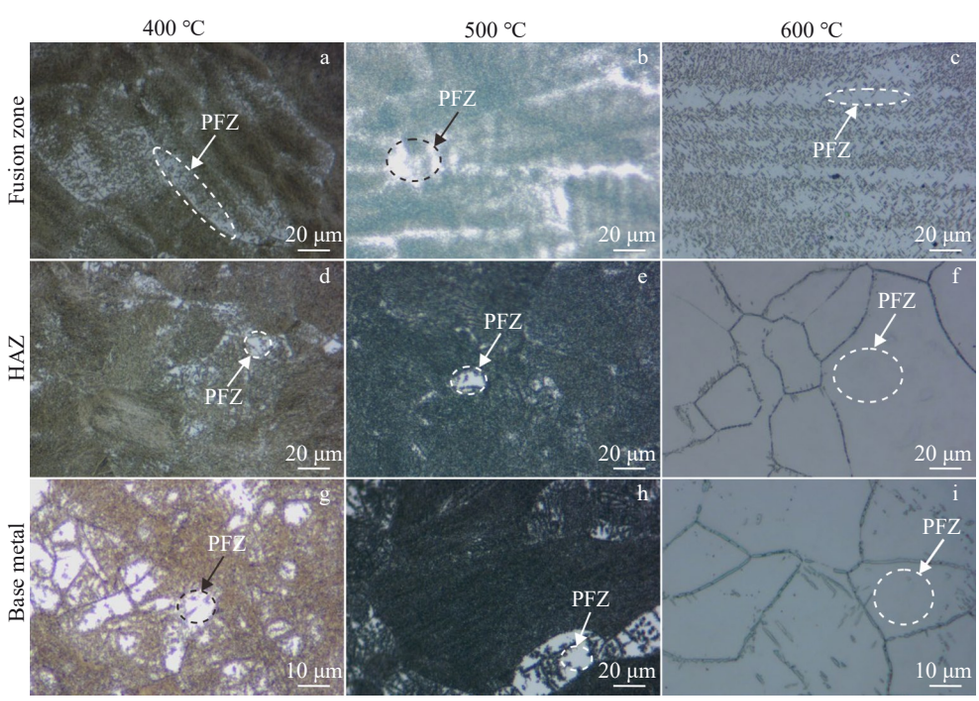

Fig.8 Morphologies of PFZs in fusion zone (a–c), HAZ (d–f), and base metal (g–i) of samples heat-treated at different temperatures for 8 h: (a, d, g) 400 ℃, (b, e, h) 500 ℃, and (c, f, i) 600 ℃

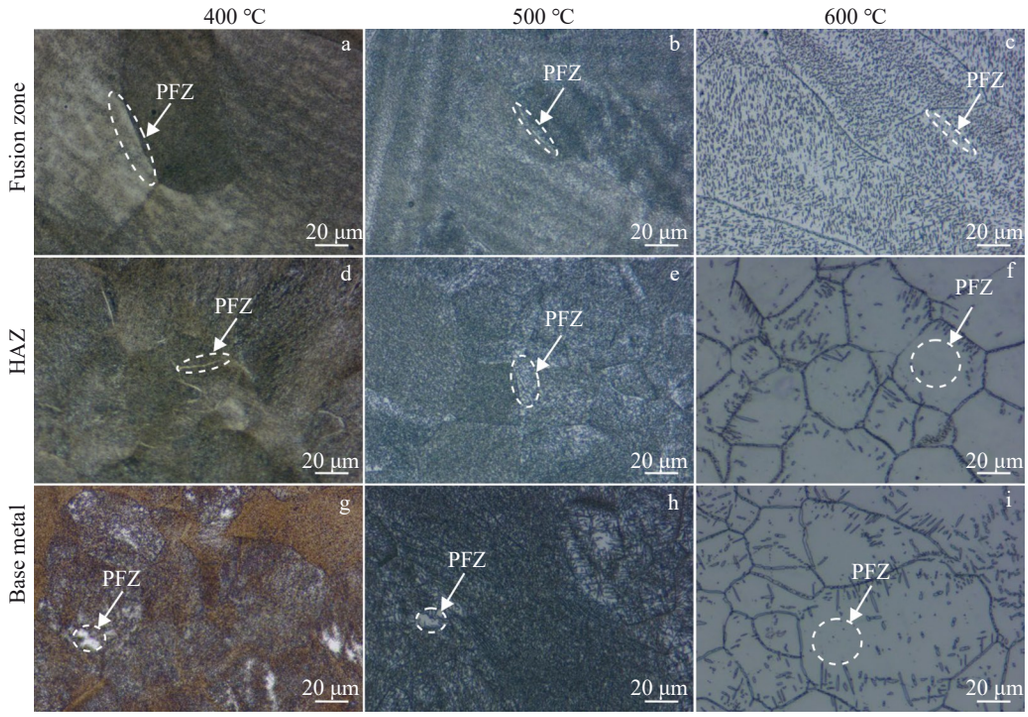

Fig.9 Morphologies of PFZs in fusion zone (a–c), HAZ (d–f), and base metal (g–i) of samples heat-treated at different temperatures for 24 h: (a, d, g) 400 ℃, (b, e, h) 500 ℃, and (c, f, i) 600 ℃

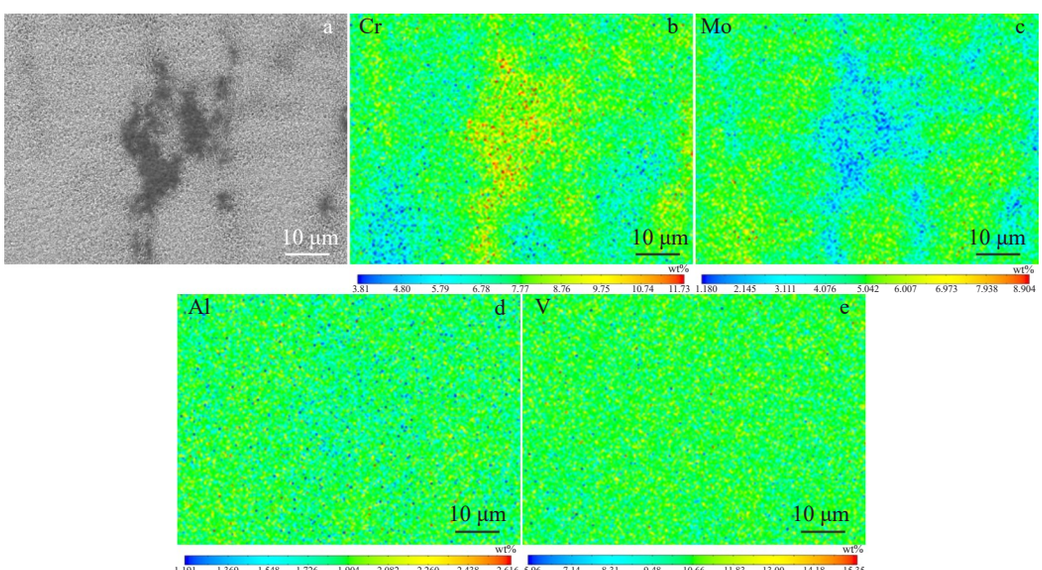

Fig. 10 Morphology of PFZs in the fusion zone of 500-8 sample (a) and corresponding EPMA element mappings (b–e): (b) Cr; (c) Mo; (d) Al; (e) V

of element Cr is lower than 1[17–18]. As a result, the element Mo tends to concentrate on the dendrite arms, while the element Cr tends to concentrate on the spacings between the dendrite arms. The element Cr has a stronger stabilizing ability than the element Mo, according to Eq. (2). The α phase is difficult to precipitate in the region with a higher content of element Cr. As a consequence, PFZs tend to form within the spacings between the dendrite arms. Similar phenomenon is also found in laser additive-manufactured β titanium alloy[19]. Therefore, the main reason for the formation of PFZs can be attributed to the segregation of elements Cr and Mo. For PFZs in HAZ and base metal, the locations are usually adjacent to the grain boundaries at which the α phase preferentially precipitates. Moreover, the α phase may also preferentially precipitate in certain areas within the grains in base metal, leading to the formation of PFZs around it, as indicated in Fig. 15b. The previous research shows that the solution treatment at temperatures higher than the β -transus temperature can increase the concentration of vacancies, which work as sites for α precipitation during the following aging treatment[20]. The concentration of vacancies in the vicinity of grain boundaries decreases because of the vacancy

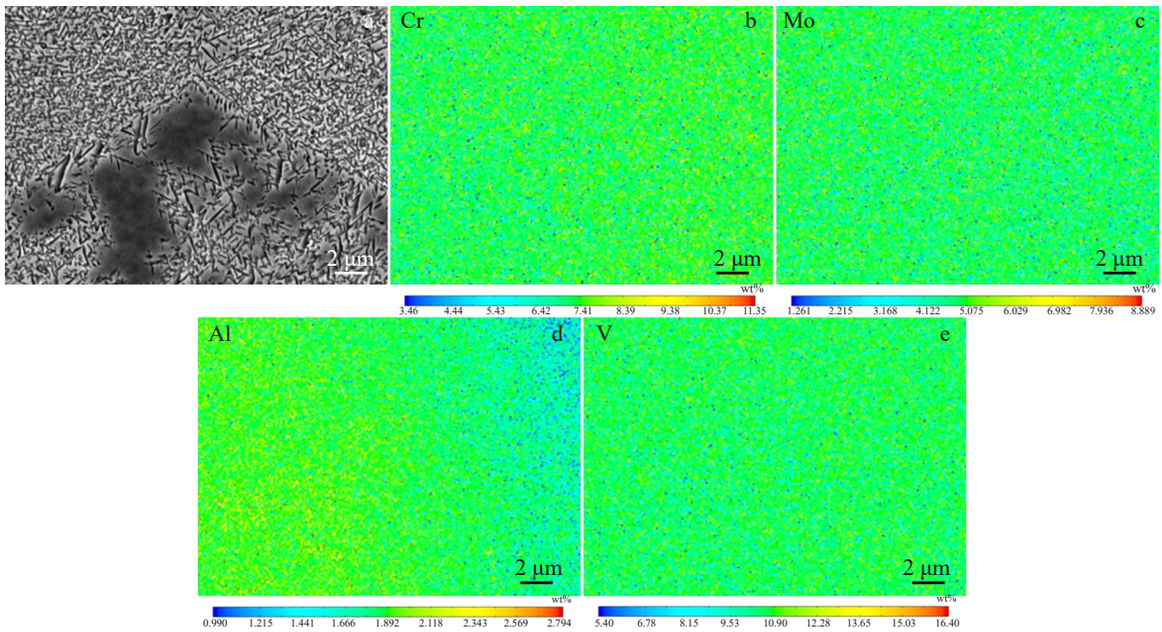

Fig.11 Morphology of PFZs in HAZ of 500-8 sample (a) and corresponding EPMA element mappings (b–e): (b) Cr; (c) Mo; (d) Al; (e) V

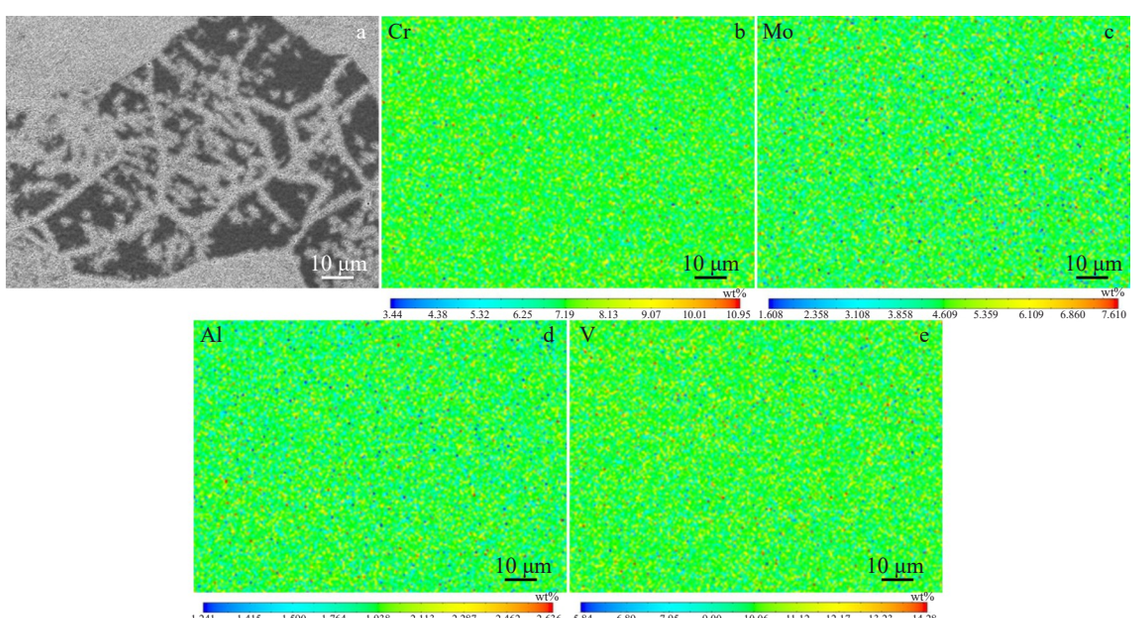

Fig.12 Morphology of PFZs in base metal of 500-8 sample (a) and corresponding EPMA element mappings (b–e): (b) Cr; (c) Mo; (d) Al; (e) V

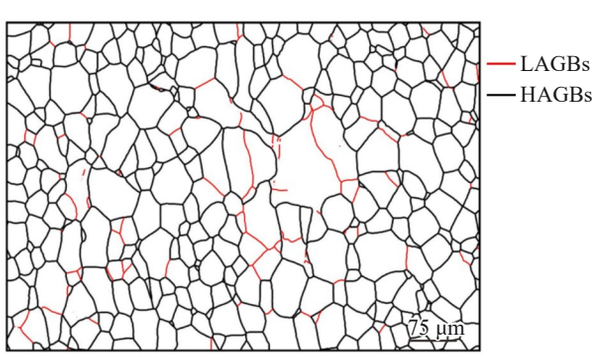

Fig. 13 Grain boundary distribution map of the base metal of 500-8 sample (HAGBs mean high angle grain boundaries)

sink effect of grain boundaries. As a consequence, PFZs form in the vicinity of the grain boundaries. For PFZs in base metal, α phase also tends to precipitate along LAGBs as well as the grain boundaries. LAGBs can work as nucleation sites for α precipitation[21]. Meanwhile, LAGBs are also vacancy sinks[22], causing a lack of nucleation sites in the vicinity of LAGBs and grain boundaries. Therefore, the main reason for the formation of PFZs in HAZ and base metal can be attributed to vacancy depletion.

This study provides a relatively confined discussion on the microstructure-property relationship. Future research will focus on investigating the influence of microstructural heterogeneity on the performance of laser welded TB9 alloys.

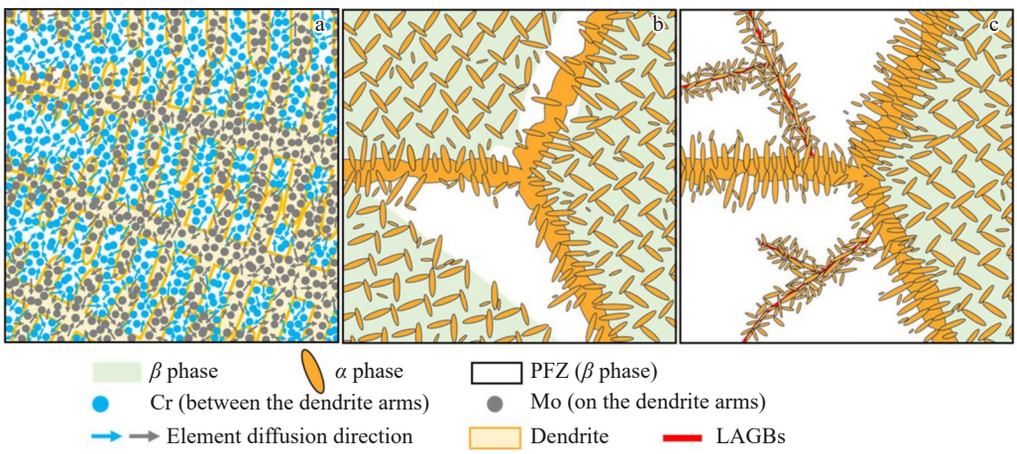

Fig.14 Schematic diagrams of the formation of PFZs in fusion zone (a), HAZ (b), and base metal (c)

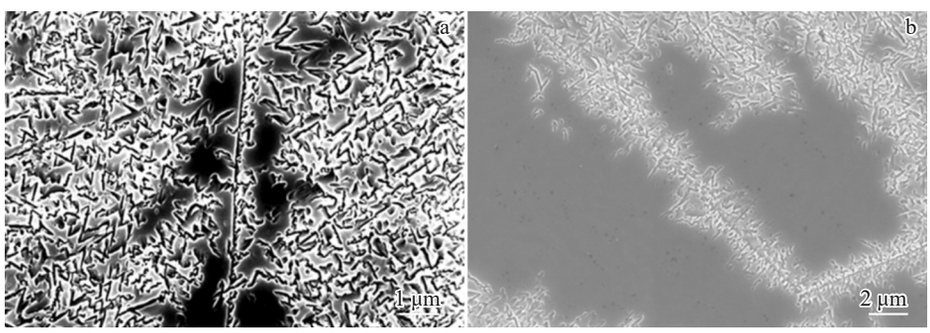

Fig.15 SEM images of PFZs in HAZ (a) and base metal (b) of 500-8 sample

4 Conclusions

1) The fusion zone of laser welded TB9 joints is composed of columnar β grains, and the size of grains increases with the increase in laser power.

2) During the aging treatment, the size of the α phase increases, while its quantity decreases with the increase in temperature.

3) PFZs are between the dendrite arms in fusion zone, while those in HAZ are near the grain boundaries. PFZs in base metal are near LAGBs and grain boundaries.

4) The primary cause of PFZs in the fusion zone is attributed to the segregation of element Cr, whereas in HAZ and base metal, it is attributed to vacancy depletion.

References

1 Williams J C, Boyer R R. *Metals*[J], 2020, 10(6): 705

2 Li Yanxing, Zhou Zhe, Wang Lin *et al*. *Rare Metal Materials and Engineering*[J], 2023, 52(3): 953 (in Chinese)

3 Liu X Y, Chu P K, Ding C X. *Materials Science and Engineering R: Reports*[J], 2004, 47(3–4): 49

4 Dalgaard E, Wanjara P, Gholipour J *et al. Acta Materialia*[J], 2012, 60(2): 770

5 Akhonin S V, Belous V Y, Berezos V A *et al. Materials Science Forum*[J], 2018, 927: 112

6 Wang G Q, Chen Z Y, Li J W *et al. Journal of Materials Science & Technology*[J], 2018, 34(3): 570

7 Shariff T, Cao X, Chromik R R *et al. Canadian Metallurgical Quarterly*[J], 2011, 50(3): 263

8 Pasang T, Amaya J M S, Tao Y *et al. Procedia Engineering*[J], 2013, 63: 397

9 Yang X W, Li W Y, Fu Y *et al. Journal of Materials Research and Technology*[J], 2019, 8(5): 4797

10 Long J, Zhang L J, Ning J *et al. Journal of Manufacturing Processes*[J], 2021, 64: 1329

11 Ren D C, Liu Y J, Zhang H B *et al. Rare Metal Materials and Engineering*[J], 2020, 49(3): 1083

12 Hu M, Qiu J K, Lei X F *et al. Journal of Aeronautical Materials*[J], 2024, 44(2): 159

13 Xu W F, Ma J, Luo Y X *et al. Transactions of Nonferrous Metals Society of China*[J], 2020, 30(1): 160

14 Ankem S, Greene C A. *Materials Science and Engineering A*[J], 1999, 263(2): 127

15 Zhang P P, Wang Q Z, Gao Q *et al. Hot Working Technology*[J], 2012, 41(14): 51

16 Huan X Y, Liu C L, Miao K S *et al. Materials Science and Engineering A*[J], 2023, 873: 145029

17 Bermingham M J, McDonald S D, StJohn D H *et al. Journal of Materials Research*[J], 2009, 24: 1529

18 Bermingham M J, McDonald S D, Dargusch M S *et al. Journal of Materials Research*[J], 2008, 23: 97
19 Ng C H, Bermingham M J, Dargusch M S. *Additive Manufacturing*[J], 2021, 39: 101855
20 Huang X, Cuddy J, Goel N *et al. Journal of Materials Engineering and Performance*[J], 1994, 3: 560
21 Zhang H, Zhang J Y, Liu S Y *et al. Acta Materialia*[J], 2023, 255: 119082
22 Yu G X, Zhao D X, Li K *et al. Materials Science and Engineering A*[J], 2022, 858: 144180

激光焊接TB9钛合金接头的显微组织演变和不均匀析出

冯静茹，张可召，刘　栋，严春妍，程江波，包晔峰
(河海大学 材料科学与工程学院，江苏 常州 213200)

摘　要：研究了激光焊接和焊后热处理过程中TB9钛合金激光焊接接头的显微组织演变规律。研究结果表明，在激光焊接过程中，随着激光功率的增大，焊缝区β相的平均晶粒尺寸增大。在焊后时效处理过程中，随着温度的升高，α相的尺寸增大，数量减少；随着时效时间的延长，α相的尺寸增大，同时，α相的形态由针状变为椭球状。焊后热处理后，焊接接头的焊缝区、热影响区（HAZ）和母材中均观察到无析出区（PFZs）存在，这主要是α相的不均匀析出和长大造成的。PFZs存在于焊缝区的枝晶臂之间，HAZ的晶界附近，以及母材的小角度晶界（LAGBs）和晶界附近。焊缝区PFZs产生的主要原因是Cr元素在枝晶臂间富集。在HAZ和母材中，PFZs的形成则是由于晶界和LAGBs附近的空位耗竭。

关键词：β钛合金；激光焊接；α相析出；无析出区

作者简介：冯静茹，女，2000年生，硕士，河海大学材料科学与工程学院，江苏 常州 213200，E-mail：fengjingru2025@163.com